Eur. Phys. J. C 40, 145–156 (2005)
Digital Object Identifier (DOI) 10.1140/epjc/s2004-02099-4

THE EUROPEAN PHYSICAL JOURNAL C

Neutrino dimuon production and the strangeness asymmetry of the nucleon

F. Olness[1], J. Pumplin[2], D. Stump[2], J. Huston[2], P. Nadolsky[1], H.L. Lai[3], S. Kretzer[4], J.F. Owens[5], W.K. Tung[2]

[1] Department of Physics, Southern Methodist University, Dallas, TX 75275, USA
[2] Department of Physics and Astronomy, Michigan State University, E. Lansing, MI 48824, USA
[3] Taipei Municipal Teachers College, Taiwan
[4] Physics Department and RIKEN-BNL Research Center, Brookhaven National Laboratory, Upton, NY 11973, USA
[5] Department of Physics, Florida State University, Tallahassee, FL 32306, USA

Received: 15 January 2004 / Revised version: 23 November 2004 /
Published online: 15 February 2005 –

Abstract. We have performed the first global QCD analysis to include the CCFR and NuTeV dimuon data, which provide direct constraints on the strange and antistrange parton distributions, $s(x)$ and $\bar{s}(x)$. To explore the strangeness sector, we adopt a general parametrization of the non-perturbative $s(x)$, $\bar{s}(x)$ functions satisfying basic QCD requirements. We find that the strangeness asymmetry, as represented by the momentum integral $[S^-] \equiv \int_0^1 x[s(x)-\bar{s}(x)]\mathrm{d}x$, is sensitive to the dimuon data provided the theoretical QCD constraints are enforced. We use the Lagrange multiplier method to probe the quality of the global fit as a function of $[S^-]$ and find $-0.001 < [S^-] < 0.004$. Representative parton distribution sets spanning this range are given. Comparisons with previous work are made.

PACS. 11.30.Hv, 12.15.-y, 13.15.+g, 12.38.-t, 13.60.Hb

1 Introduction

The recent measurements of both neutrino and antineutrino production of dimuon final states (charm signal) by the CCFR and NuTeV collaborations [1] provide the first promising direct experimental constraints on the strange and antistrange quark distributions of the nucleon, $s(x)$ and $\bar{s}(x)$. In addition to the intrinsic interest in the nucleon structure [2], the strange asymmetry $(s-\bar{s})$ has important implications on the precision measurement of the Weinberg angle in deep inelastic scattering of neutrinos [3–8]. We report here the first global QCD analysis that includes the new dimuon data, using the methods developed by the CTEQ collaboration, specifically to explore the strange and antistrange parton parameter space.[1]

In previous global analyses, information on s and $\bar{s}$ has resided only in inclusive cross sections for neutral and charged current DIS. The reliability of the extraction of the quite small s and $\bar{s}$ components[2] (from differences of large cross sections measured in different experiments) was always in considerable doubt. For this reason, most global fits adopted the assumption $s(x) = \bar{s}(x) = \kappa(\bar{u}+\bar{d})/2$; this approximation was inferred from the earlier combined neutrino and antineutrino dimuon experiments [11] which extract a consistent value of

$$\kappa \equiv \frac{\int \mathrm{d}x\; x\left[s(x,Q^2)+\bar{s}(x,Q^2)\right]}{\int \mathrm{d}x\; x\left[\bar{u}(x,Q^2)+\bar{d}(x,Q^2)\right]} \sim 0.4 \qquad (1)$$

at some low value of Q. The recent high-statistics dimuon measurements of [1] provide greater accuracy, and the high purity of separate neutrino and antineutrino events offers the first opportunity to study the difference $s(x)-\bar{s}(x)$. Neutrino induced dimuon production, $(\nu/\bar{\nu})N \to \mu^+\mu^- X$, proceeds primarily through the subprocesses $W^+ s \to c$ and $W^-\bar{s} \to \bar{c}$ respectively, and hence provides independent information on s and $\bar{s}$.

We present the first global QCD analysis that includes these new dimuon data. The new results demonstrate, first of all, that the strangeness asymmetry, as measured by the momentum integral

$$[S^-] \equiv \int_0^1 x[s(x)-\bar{s}(x)]\mathrm{d}x\ , \qquad (2)$$

is indeed more sensitive to the dimuon data than to the other DIS data. We then use the recently developed Lagrange multiplier method of global analysis to explore the range of uncertainty of $[S^-]$. In this first report, we concentrate on $[S^-]$, the integrated strangeness asymmetry,

[1] A preliminary version of this study was reported at the Lepton Photon 2003 International Symposium (LP2003), Fermilab, August 2003. Cf. Gambino [9] and Thorne [10], published in the Proceedings of LP2003.

[2] The strangeness content of the nucleon, as measured by the momentum fraction carried by s or $\bar{s}$, is of order 3% at $Q = 1.5\,\mathrm{GeV}$.

which represents a new parton degree of freedom in the nucleon heretofore largely unexplored, and which has immediate impact on precision electroweak physics because of the NuTeV anomaly [3]. A full exploration of the density functions $s(x)$ and $\bar{s}(x)$ will be presented later.

We begin by describing the general features of the strangeness sector of the nucleon structure in the QCD framework and our general parametrization of that sector. A brief review and discussion of the pQCD calculations that are relevant to the interpretation of the dimuon data is then followed by the main results of the global analysis, with emphasis on concrete representative global fits relevant for probing the strangeness asymmetry and on Lagrange multiplier results for the integrated momentum asymmetry (2). This paper concludes with a summary of the extensive studies performed beyond the examples given, comparisons to previous work on strangeness asymmetry, and conclusions.

2 General properties of $s(x) - \bar{s}(x)$ and its first two moments

Before we discuss the concrete fitting procedure and the results in the following sections, we feel that it is instructive to formulate the qualitative expectations that are based on general QCD requirements (before any data).

2.1 Requirements

For each Q, let us define the strangeness *number densities* $s^{\pm}(x)$ and their integrals $[s^{\pm}]$ by

$$[s^{\pm}] \equiv \int_0^1 s^{\pm}(x)\,\mathrm{d}x \equiv \int_0^1 [s(x) \pm \bar{s}(x)]\,\mathrm{d}x\,, \qquad (3)$$

and the *momentum densities* $S^{\pm}(x)$ and integrals $[S^{\pm}]$ by

$$[S^{\pm}] \equiv \int_0^1 S^{\pm}(x)\,\mathrm{d}x \equiv \int_0^1 x[s(x) \pm \bar{s}(x)]\,\mathrm{d}x\,. \qquad (4)$$

In the QCD parton model, certain features of these quantities are necessary.
(1) The parton distributions $s(x,Q^2)$ and $\bar{s}(x,Q^2)$[3] [or equivalently $s^{\pm}(x)$], are parametrized at some low (but still perturbative) scale Q_0; the full Q-dependence is then determined by DGLAP evolution.[4]
(2) The strangeness number sum rule for the nucleon requires

$$[s^-] = 0 \qquad (\text{for all } Q). \qquad (5)$$

A necessary corollary is that the density function $s^-(x)$ must be less singular than $1/x$ as $x \to 0$ for all Q. As DGLAP evolution preserves (5) (which is a consequence of the conservation of the strange vector current $J_s^\mu = \bar{\psi}_s \gamma^\mu \psi_s$), it suffices to impose it at Q_0.
(3) The momentum sum rule requires

$$[S^+] = 1 - \Sigma_0 \qquad (\text{for all } Q), \qquad (6)$$

where Σ_0 represents the momentum fraction of all non-strange partons. Through this condition the global inclusive DIS and other data – which directly affect Σ_0 – indirectly also constrain $[S^+]$.
(4) In the limit $x \to 0$ (high energy and fixed Q), Regge considerations and the Pomeranchuk theorem predict

$$s^-(x)/s^+(x) \to 0\,.$$

2.2 Expectations

From the above general constraints, we draw the following conclusions.
(i) The number sum rule, (5), implies that a graph of $s^-(x)$ must cross the x-axis *at least once* in the interval $0 < x < 1$; and the areas bounded by the curve above and below the x-axis must be equal.
(ii) Assuming a simple scenario in which there is – as supported by theoretical models [2] based on Λ–K fluctuations – only one zero crossing, either $s^-(x) < 0$ in the low x region and $s^-(x) > 0$ in the high x region, or vice versa. The two possibilities imply $[S^-] > 0$ or $[S^-] < 0$, respectively, because the momentum integral suppresses the small x region and enhances the large x region.
(iii) The low x behavior of $|s^-(x)| \sim x^{\beta-}$ will then be correlated with the size of $|[S^-]|$: The steeper the function $s^-(x)$, the larger $|S^-(x)|$ has to be at large x.

To illustrate point (ii), we preview a representative CTEQ fit (to be discussed in full detail in Sect. 4) in Fig. 1 and juxtapose it with results from previous literature. According to the parametrizations of $s(x)$ and $\bar{s}(x)$ used by the CCFR-NuTeV dimuon study [1,12], $s^-(x)$ is negative in the x range covered by the experiment ($0.01 < x < 0.3$).[5]

A previous detailed global analysis of inclusive data by Barone et al. [4] (BPZ), finds that $s^-(x)$ is positive in the large x region. These previous results are shown in Fig. 1 as the dot-dashed and dashed curves, respectively. In light of the theoretical constraints discussed above, both these results would hint at the first possibility mentioned above, i.e. $[S^-] > 0$. This is not the case, however, for the CCFR-NuTeV curve, as it does not cross the x-axis; it violates the strangeness number sum rule and cannot be taken to represent the physics outside a limited window in x. The BPZ curve does satisfy the sum rule; we note (Fig. 1) that it has two zero-crossings. The solid curves (Class B) in the two plots of Fig. 1 provide a concrete example of $s^-(x)$ and $S^-(x)$ following the above requirements and expectations.

[3] As we had done already in (3) and (4) above, we will suppress the obvious Q^2 dependence from now on.

[4] For definiteness, the CTEQ PDFs evolve from $Q_0 = m_c = 1.3\,\mathrm{GeV}$.

[5] Since the preliminary version of this work was reported, the CCFR-NuTeV collaboration has emphasized that their most recent analysis favors an integrated strangeness asymmetry that is consistent with zero [28]. More definitive studies are needed to clarify the situation. See further discussions in Sect. 5.

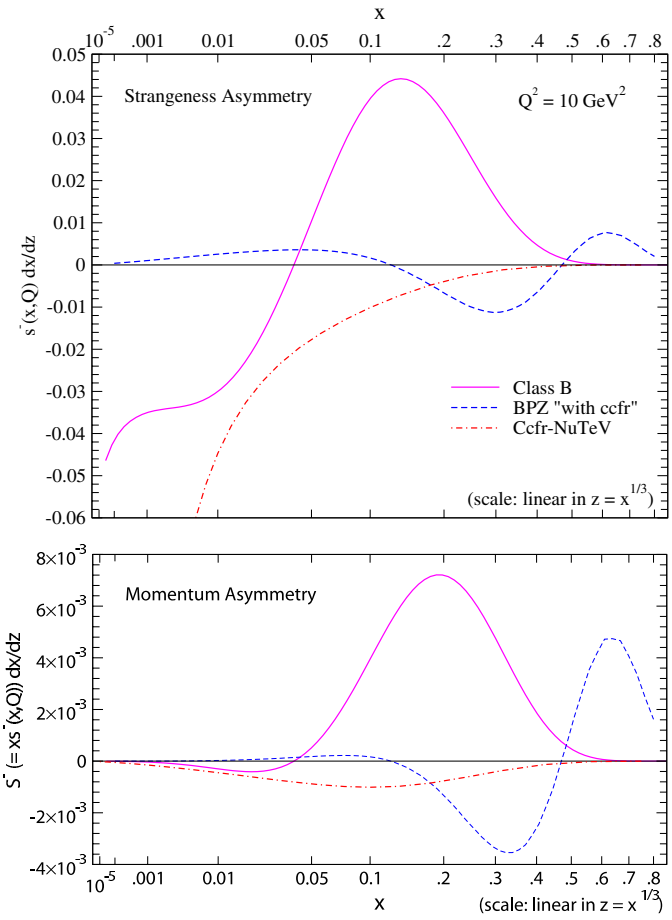

Fig. 1. Different functional behaviors of the strangeness number asymmetry function $s^-(x)$ and momentum asymmetry function $S^-(x)$: comparison of our central fit "B" (solid, discussed in detail later in the text) with those of BPZ (dashed) and CCFR-NuTeV (dot-dashed). The horizontal axis is linear in $z \equiv x^{1/3}$ so that both large and small x regions are adequately represented; the functions are multiplied by a Jacobian factor $\mathrm{d}x/\mathrm{d}z$ so that the area under the curve is the corresponding integral over x

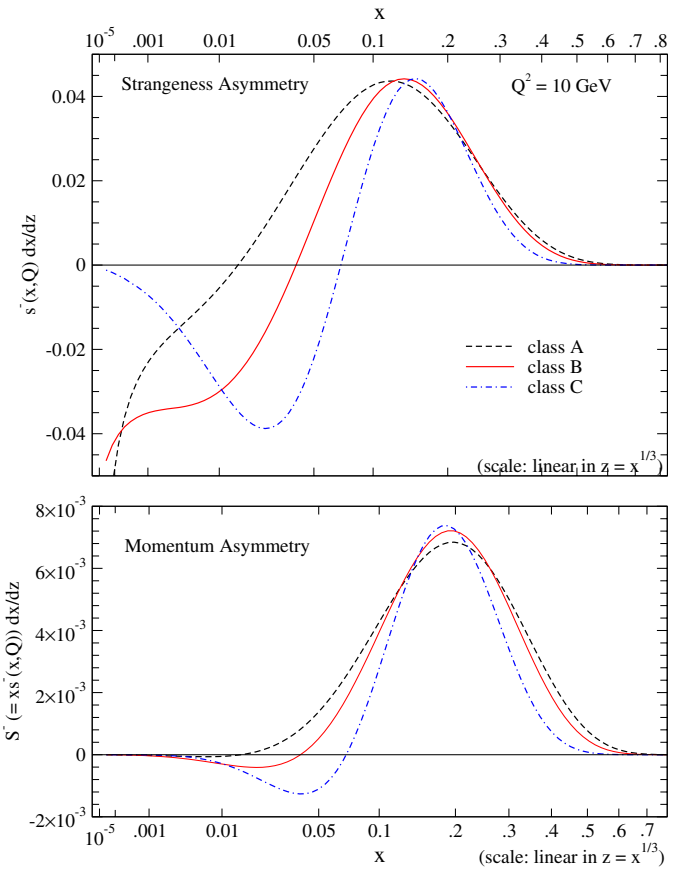

Fig. 2. Typical strangeness asymmetry $s^-(x)$ and the associated momentum asymmetry $S^-(x)$, as obtained in our global analysis. The axes are the same as in Fig. 1

To illustrate point (iii), we preview various classes of solutions (again, to be discussed in detail below) in the upper plot of Fig. 2. Because the experimental constraints are weak or non-existent in the very small x region, say $x < 0.01$, the detailed behavior of $s^-(x)$ is unconstrained in this region. However, this uncertainty at small x is considerably reduced in $S^-(x)$, as demonstrated by the curves of the lower plot. Thus the above observations concerning $[S^-]$ are affected only mildly by the uncertainty of the very small x behavior, unless that behavior is so extreme that the small x region provides a significant contribution to the number sum rule. We will refrain from exploiting such a mathematical possibility as long as it does not seem to be motivated by any physics.[6]

3 General parametrization of the strangeness distributions

To explore the strangeness sector of the parton structure of the nucleon, we need a suitable parametrization of $s(x)$ and $\bar{s}(x)$ (or equivalently $s^{\pm}(x)$) at a fixed scale Q_0. This parametrization must satisfy the theoretical requirements specified above, and it should be as general as possible so that the allowed functional space can be fully explored. A general form is essential, so that our conclusions are not artifacts of the parametrization, but truly reflect the experimental and theoretical constraints. In the following we explain our choice of such a parametrization. Full details including explicit parameters are given in the appendix.

It is more natural to parametrize the $s^{\pm}(x, Q_0)$ functions independently (rather than s and $\bar{s}$) since they satisfy different QCD evolution equations: pure non-singlet for s^- and mixed singlet/non-singlet for s^+. We use the following parametrizations:

$$s^+(x, Q_0) = A_0\, x^{A_1}(1-x)^{A_2} P_+(x; A_3, A_4, \ldots), \qquad (7)$$

[6] A residual bias of the results on the assumed functional forms, or rather on the rejection of some forms as merely mathematical and not physical, is unavoidable in parton analyses. One can imagine the extreme (unphysical) scenario of spike-like structures escaping "detection" in the $x \to 0$ region but, nevertheless, affecting sum rules.

$$s^-(x,Q_0) = s^+(x,Q_0) \times \tanh[a\,x^b(1-x)^c P_-(x;x_0,d,e,\ldots)], \quad (8)$$

where $P_+(x;A_3,\ldots)$ is a positive definite, smooth function in the interval $(0,1)$, depending on additional parameters $A_3,\ldots$ such as are used for $u,d,g,\ldots$ in most CTEQ [13] and other global analyses [14,15], and

$$P_-(x) = \left(1-\frac{x}{x_0}\right)\left(1+dx+ex^2+\ldots\right), \quad (9)$$

where the crossing point x_0 is determined by the strangeness number sum rule $[s^-]=0$, and the parameters $d,e,\ldots$ are optional, depending on how much detail is accessible with the existing constraints. Important features of this parametrization are the following.
(1) The strangeness quantum number sum rule, $[s^-]=0$, is satisfied by the choice of x_0. The parameter x_0 has a physical interpretation: it is the "crossing point" where $s^-(x)=0$. (If d and/or e are not zero, there can be additional zeros of $s^-(x)$; in practice – as explained in the previous section and below in Sect. 4.2 – we restrict our analysis to solutions with a single crossing only.)
(2) The fact that the tanh function has absolute value less than 1 ensures positivity of $s(x)$ and $\bar{s}(x)$. The fact that tanh is a monotonic function guarantees that the function $s^-(x)$ can be made as general as necessary by the choice of $P_-(x)$.
(3) The small x behavior of $s^-(x)$ must be such that the integral $[s^-]$ converges (before the root x_0 is determined). Let $\beta_- \equiv A_1 + b$; then (8) implies

$$s^-(x) \sim x^{\beta_-} \text{ as } x \to 0. \quad (10)$$

The convergence of $[s^-]$ is guaranteed if $\beta_- > -1$, i.e. the parameter b is chosen in the range $b > -1 - A_1$.

Because $P_\pm(x)$ can be made as general as necessary, the choice in (7)– (9) is capable of exploring the full strangeness parameter space allowed by the data in the pQCD framework.

Detailed formulas for all flavors used in the actual analysis are presented in the appendix.

4 Global analysis

We now describe the global QCD analysis, which includes all relevant experimental data and implements the theoretical ideas outlined above. This may be considered an extension of the on-going CTEQ program of global analysis. Several new elements (compared to the latest CTEQ6M [13] analysis) are present. On the experimental side, we have added the CDHSW inclusive F_2 and F_3 data sets [16], and the CCFR-NuTeV dimuon data sets [1]. On the theoretical side, we have expanded the parameter space to include the strangeness sector as discussed in Sect. 3.

Compared to the global analyses of BPZ [4], which also allow for $s \neq \bar{s}$, the major difference experimentally is our inclusion of the dimuon data, which provide a direct handle on s and $\bar{s}$, and, theoretically, the generality and naturalness of our parametrization of the strange distributions.[7] Since the results of [4] on the strangeness asymmetry rely on small differences of the inclusive DIS charged-current and neutral-current measurements, BPZ performed the analysis at the cross section level, applying uniform procedures to treat data from different experiments in the comparison to theory. Considering small differences between inclusive cross sections, the possible strange asymmetry is but one of many sources that could lead to such differences.

As the dimuon data more directly constrain the strange PDFs, this is an important new element to our fit. For all inclusive DIS processes we use the standard procedure of comparing theory with the published F_2 and F_3 structure function data. In our analysis, the fit to charged-current (neutrino) inclusive structure functions is dominated by the high statistics CCFR data. Although we have included the earlier inclusive CDHSW data (which play a prominent role in the analysis of [4]), they have no discernible influence on the results presented below.

To include the CCFR-NuTeV neutrino and antineutrino dimuon production data in a global QCD analysis is not a straightforward task. The experimental measurement is presented as a series of *forward differential cross sections* with kinematic cuts, whereas the theoretical quantities that are most directly related to the parton distribution analysis are the underlying (semi-) inclusive *charm quark production cross sections*. The gap between the two is bridged using a Monte Carlo program that incorporates kinematic cuts as well as fragmentation and decay models. In our analysis, we use a Pythia program provided by the CCFR-NuTeV collaboration to do this efficiency correction.[8] This Monte Carlo calculation is done in the spirit and the framework of leading-order (LO) QCD. CTEQ5L parton distributions and Peterson fragmentation functions were used. The parameters of the model were tuned to reproduce, as closely as possible, the detailed differential dimuon cross sections published in [1].

4.1 $\mathrm{d}\sigma^{\nu n\to cx}$ in QCD

At LO in pQCD, the cross section formula for $\nu N \to cX$ is [17]

$$\xi s'(\xi,Q^2)_{\text{eff}} \equiv \frac{1}{2}\,\frac{\pi(1+Q^2/M_W^2)^2}{G_{\text{F}}^2 M_N E_\nu}\,|V_{cs}|^{-2}\,\frac{\mathrm{d}^2\sigma^{\nu N\to cX}}{\mathrm{d}x\,\mathrm{d}y} = \left(1-\frac{m_c^2}{2M_N E_\nu \xi}\right)\,\xi s'(\xi,Q^2)+\mathcal{O}(\alpha_{\text{s}}), \quad (11)$$

with the CKM matrix element $|V_{cs}|$ and where the Barnett–Gottschalk parameter [18,19]

$$\xi \equiv x\,\left(1+\frac{m_c^2}{Q^2}\right) \quad (12)$$

[7] Reference [4] parametrizes $s(x)$ and $\bar{s}(x)$ rather than $s^\pm(x)$.
[8] We thank Tim Bolton and Max Goncharov, in particular, for providing this program, as well as assistance in its use. Their help was vital for carrying out this project.

approaches the Bjorken variable x as $Q \to \infty$ (relative to $m_c = 1.3$ GeV). The quantity $s'(\xi, Q^2)_{\rm eff}$ in (11) includes Cabibbo suppressed contributions in neutrino scattering via

$$s' \equiv s + \frac{|V_{cs}|^2}{|V_{cd}|^2}\, d, \tag{13}$$

with obvious adjustments for the antineutrino case.[9]

The NLO corrections to $\xi s'(\xi, Q^2)_{\rm eff}$, defined via the perturbative series

$$\xi s'(\xi, Q^2)_{\rm eff} = \sum_i \alpha_{\rm s}^i \; \xi s'(\xi, Q^2)^{(i)}_{\rm eff} \;, \tag{14}$$

are generically of the form

$$\xi s'(\xi, Q^2)^{(1)}_{\rm eff} \propto \sum_{f=g,s'} f \otimes H_f, \tag{15}$$

with $\otimes$ denoting a convolution integral over parton momentum. These were first calculated more than 20 years ago [19]. Later calculations [17, 20] corrected minor typos and employed the modern $\overline{\rm MS}$ renormalization scheme and the ACOT treatment [21] of amplitudes with massive quarks ($m_{s,c} \neq 0$). Very recently, the NLO charm production contributions to the full set of electroweak structure functions were calculated [22], including terms that are suppressed by m_μ^2/ME_ν. In order to apply detector acceptance corrections to the data [1], differential NLO distributions were calculated in [23, 24] that provide the charm hadron (D meson) kinematics in terms of the fragmentation variable z and rapidity η. The $\mathrm{d}\sigma/\mathrm{d}x\mathrm{d}y\mathrm{d}z\mathrm{d}\eta$ code DISCO [24], written by two of the authors of the present article in collaboration with D. Mason of NuTeV, exists as an interface to the NuTeV MC event generator. Detailed results can be found in the articles listed above. It suffices to say that
(i) the NLO calculations all agree, and
(ii) for the fixed target kinematics under investigation, the NLO corrections to the LO results are modest – no bigger than $\lesssim 20\%$ (see Fig. 1 in [17]).

As mentioned before, the global fits performed in our study are extensions of the full NLO CTEQ6 analysis with the addition of constraints due to neutrino dimuon production. For the latter process, we have done extensive studies using either the LO formula, (11), or the NLO treatment of [17], (15). The results obtained in the two cases are quite similar. For definiteness, the main results presented in Sect. 4.3 are those obtained by using (11), since the acceptance corrections made to the data set are currently based on a LO model, as mentioned earlier. Since we have determined that the NLO corrections to the hard cross section are small (compared to the experimental errors, for instance), and since we found the uncertainty range of the main result (on $[S^-]$) is much broader than the difference between the central values obtained by using (11) with or without the corrections in (15) (cf. Sect. 5), this approximation does not affect the outcome of our analysis.[10]

[9] $q \to \bar{q}$ for $q = s, d$.

[10] It is certainly desirable to have the inclusive cross sections corrected for acceptance based on NLO models (such as [24]), that can be compared to (15) in a full NLO global analysis. This is under active development by a theory (CTEQ)–experiment (CCFR-NuTeV) collaboration.

4.2 Procedure

Our analysis is carried out in several stages. First we must find appropriate starting values for the fitting parameters. For this purpose, we implement the following steps.
(1) We rerun the CTEQ6M global fit with the added CDHSW inclusive neutrino scattering data, keeping all other conditions the same. This intermediate fit is extremely close to the CTEQ6M one, since the fit to inclusive DIS data is totally dominated by the high statistics neutral current experiments on the one hand and the CCFR charged current experiment on the other.
(2) We then fix all of the *conventional* parton parameters to their values in this intermediate fit, and fit the complete set of data, including the new dimuon data, by varying only the parameters associated with the new degrees of freedom in s^-. We obtain results consistent with expectations.
(i) Most of the data sets used in the previous analysis are not affected at all by the variation in s^-.
(ii) A few fully inclusive cross sections are slightly affected by the variation of s^-; mainly
(a) F_3 which depends on $u - \bar{u} + d - \bar{d} + s - \bar{s}\ \ldots$;
(b) the $W^\pm$ charge asymmetry which receives a contribution from $gs \to W^- c$. The sensitivities to s^- are weak.
(iii) The CCFR-NuTeV dimuon data sets are the most constraining ones for fitting $s^-(x)$.

We obtain good fits using either the 3-parameter (a, b, c) or the 4- or 5-parameter (a, b, c, d, e) versions of (8) and (9). There are not enough constraints to choose among these fits. The higher-order polynomials allow oscillatory behavior of $s^-(x)$ which the 3-parameter form does not. We consider the number of crossings a distinctive property of the physical asymmetry $s^-(x)$ rather than a volatile function of the continuous fit parameter space. As explained in Sect. 2, one zero-crossing is unavoidably enforced by the sum rule in (5). We are not aware of any solid theoretical argument that would suggest a second crossing; nor do we find that the fits show any preference for more than one crossing. We therefore restrict the search for best fits in this section to one crossing. This choice also seems to be a stable feature of models [2] based on baryon–meson fluctuations.
(3) Using these candidate fits as a basis, we perform a second round of fitting allowing the parameters associated with s^+, (7), to vary in addition to the s^- variables. This improves the fit to all data sets slightly. We observe that the shape of $s^+(x)$ now deviates from the starting configuration in which $s^+(x)$ was set proportional to $\bar{u}(x) + \bar{d}(x)$. Defining, as in (1), the strangeness suppression parameter κ as the ratio of the momentum fraction carried by the strange quarks, $[S^+]$, to that carried by $\bar{u} + \bar{d}$ at $Q_0 = 1.3\,\mathrm{GeV}$, we find that κ may vary in the range 0.3–0.5: χ^2 has a shallow minimum around $\kappa = 0.4$. This value agrees with previous analyses [11].

Because the experimental constraints are not sufficient to uniquely determine all the s^- and s^+ parameters, we

categorize several classes of equally good solutions based on the behavior of $s^-(x)/s^+(x)$ as $x \to 0$ or $x \to 1$.
(4) We finalize these classes of solutions by allowing all parton parameters to vary so that the non-strange parton distributions can adjust themselves to yield the best fit to all the experimental data sets. (As one would expect, these final adjustments are generally small.) The differences in the χ^2 values between the various categories of solutions are not significant; i.e. we find nearly degenerate minima with distinctively different $s^-(x)$ solutions, classified according to their small x behavior. These solutions do not correspond to isolated local minima in χ^2 space; rather they are to be thought of as specific examples of a class of acceptable fits that lie along a nearly flat "valley" along which χ^2 changes very slowly.

4.3 Central results

The quality of the fits to the global data sets other than the CCFR-NuTeV dimuon data remains unaltered from the previous CTEQ6M analysis, so we focus our discussion on the strangeness sector. Specifically, we examine closely the asymmetry functions $s^-(x)$, $S^-(x)$ and the momentum integral $[S^-]$. The asymmetry functions from three typical good fits, with different behaviors at small x (labeled as classes A, B, C), were previewed in Fig. 2 as illustrations.

In the accompanying table, Table 1, for each sample fit we list the small x exponent β_- [$s^-(x) \sim x^{\beta_-}$, cf. (10)], the integrated momentum fraction $[S^-]$, and the relative χ^2 values, normalized to the χ^2 of solution B (χ^2_B), which we use as the reference for comparison purposes. (Under column "B", we give the absolute χ^2's in parentheses.[11]) To gain some insight on the constraints on the strangeness sector due to the various types of experiments, we show separately the χ^2 values for the dimuon data sets, the inclusive data sets (I) that are expected to be somewhat sensitive to s^- (consisting of the CCFR and CDHSW $F_3(x,Q)$ and the CDF W-lepton asymmetry measurements), and the remaining data sets (II) that are only indirectly affected by s^- (the rest of the inclusive data sets).

Focusing on the three good fits {A, B, C} first, we note the following features.
(1) All three solutions {A, B, C} feature positive $[S^-]$; and the more singular the behavior of $s^-(x)$ as $x \to 0$, the higher the value of $[S^-]$. These are natural consequences of the strangeness sum rule (equal $+/-$ areas under the curve of $s^-(x)$) and the small x suppression of the momentum integral, as discussed earlier in Sect. 2.
(2) Solution B is slightly favored over the other two. This, plus the fact that its small x behavior lies in the middle of the favored range, motivates its use as the reference fit.
(3) We chose these examples among fits with the simplest parametrizations: all cross the x axis only once. With four or five parameters, which can allow for more than one crossing point, many solutions can be found that entail an oscillatory $s^-(x)$. But since the χ^2 values are essentially the same as for the simple case, we deem it premature to dwell on complicated behaviors, which may be mere artifacts of the parametrization rather than reflections of physical constraints. Further studies described in Sect. 4.5 reinforce this point.

To show how these fits compare with the data, we plot in Fig. 3 the ratio of data/theory for the reference fit B. The four graphs correspond to the CCFR and NuTeV neutrino and antineutrino data sets respectively. The data points are sorted in x-bins, and within each x-bin, by y value. We see that the quality of the fit is good, within the experimental uncertainties. There are no significant systematic deviations. (The CCFR antineutrino data set may appear to be systematically higher than theory. However, upon closer inspection the difference is not significant. The data points that lie above theory consist mostly of points with large error bars, which tend to catch the attention of the eye; whereas the fit is actually dominated by points with small errors, which closely bracket the theory line on both sides.[12] The value of χ^2/N for this data set is less than 1, comparable to those for the other sets.)

The parameters for all the fits described in this section are given in detail in the appendix. As is already obvious from Fig. 2, solutions with nearly degenerate χ^2 may correspond to parametrizations of $s^-(x)$ with quite different parameter values, so that a simple linear error analysis cannot be applied. This reflects the fact that $s^-(x)$ is not well determined as a detailed function of x, even when the dimuon data are included in the fit. On the other hand, reducing the parameter space to even fewer parameters than our minimal set would risk introducing artifacts of an inflexible parametrization. In the next section we will, therefore, apply the Lagrangian multiplier method to deduce the integrated momentum asymmetry $[S^-]$ and its uncertainty.

4.4 Range of $[S^-]$ by the Lagrange multiplier method

Beyond the best fits (A, B, C), we can study the range of $[S^-]$ consistent with our global analysis in a quantitative way by applying the Lagrange multiplier (LM) method developed in [25]. By varying the Lagrange multiplier parameter, this method explores the entire strangeness parameter space in search of solutions with specified values of $[S^-]$, i.e., constrained fits. The B^- solution listed in Table 1 was obtained by forcing $[S^-] = -0.0018$ (a relatively large negative value, but not as large as the value -0.0027 quoted by [6,12]). The B^+ solution was generated by forcing $[S^-]$ to go in the other (positive) direction until the increment of the overall χ^2 became comparable to that of B^-; this results in $[S^-] = 0.0054$.

[11] The χ^2 values of the dimuon data sets, like those of some other data sets, do not carry rigorous statistical significance, because the correlated systematic errors are not available and, hence, cannot be included. In the global analysis context, the χ^2 value is nevertheless used as the only practical "figure of merit" for the fit. The relatively small value of the total χ^2 for the dimuon data sets, compared to the number of data points, underlines this fact. Under this circumstance, it is common practice to use the normalized χ^2 values to compare the quality of different fits.

[12] This becomes apparent if the data points are re-plotted ordered by the size of the error bars.

Table 1. The representative parton distribution sets, arranged in order by the value of $[S^-]$

	# pts	B^+	A	B	C	B^-
β_-	–	−0.78	−0.99	−0.78	0	−0.78
$[S^-] \times 100$	–	0.540	0.312	0.160	0.103	−0.177
Dimuon	174	1.30	1.02	*1.00* (126)	1.01	1.26
Inclusive I	194	0.98	0.97	*1.00* (141)	1.03	1.09
Inclusive II	2097	1.00	1.00	*1.00* (2349)	1.00	1.00

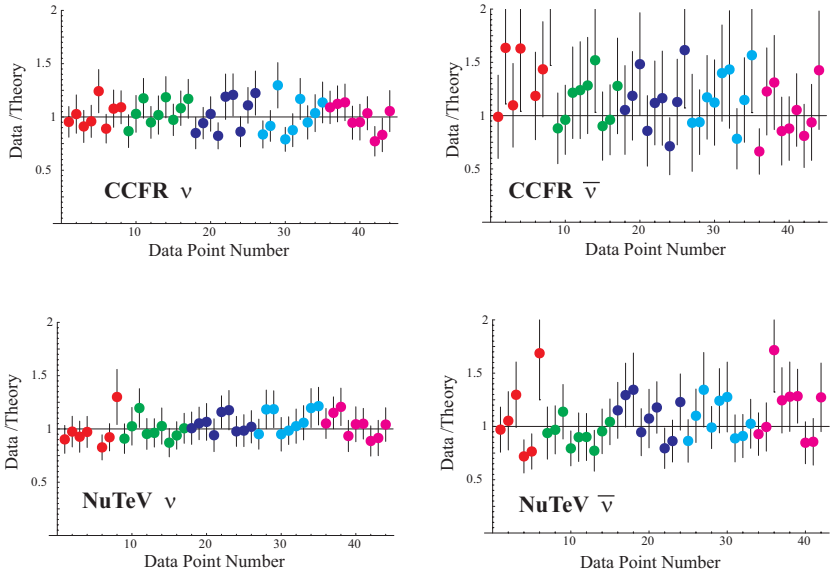

Fig. 3. Comparison of the data to fit B. The data points are sorted in x-bins, and within each x-bin, by y value. The CCFR ν and $\bar{\nu}$ data span kinematic ranges $0.023 < x < 0.336$, $0.320 < y < 0.795$ and $0.018 < x < 0.21$, $0.355 < y < 0.802$ respectively. The NuTeV ν and $\bar{\nu}$ data span kinematic ranges $0.021 < x < 0.324$, $0.334 < y < 0.79$ and $0.016 < x < 0.211$, $0.356 < y < 0.788$ respectively

We see from the relevant entries in Table 1 that (i) the χ^2 values of the dimuon data sets increase by about 30% in both $B^{\pm}$ fits; (ii) the "inclusive I" data sets disfavor the negative $[S^-]$, and (iii) the "inclusive II" data sets are completely neutral. These results are shown graphically in Fig. 4a, where the square points represent the (relative) χ^2 values of the dimuon data sets, and the triangle points of the "inclusive I" data sets. (Not shown are those for the "inclusive II" data sets, which remain flat (at 1.00).) The LM fits are chosen from a large number of fits spanning the entire strangeness parameter space. The pattern of dependence of the χ^2 values for the dimuon data sets on the value of $[S^-]$ is nearly parabolic. This is clear evidence that the dimuon measurement is indeed sensitive to the strangeness asymmetry as expected. Further discussion of this observation, including the contrast to the sensitivity of other experiments, will be given in Sect. 4.5.

We see from Fig. 4a that, in this series of fits, the dimuon data sets favor a range of $[S^-]$ centered around 0.0017, whereas the "inclusive I" data sets disfavor negative values of $[S^-]$. Figure 4b shows the dependence of the combined χ^2 of the two categories of data sets on $[S^-]$. (The χ^2 of the remaining data sets used in the global analysis are totally insensitive to $[S^-]$, cf. Table 1, hence is not included in this plot.) We would like to determine a "range of uncertainty" of $[S^-]$ from these results. This is far from straightforward because of well-known problems shared by all error assessments in global analysis (mainly due to the unquantified systematic errors that show up as a lack of statistical compatibility among the input data sets).[13]

One naive method is to apply the $\Delta\chi^2 = 1$ criterion. From the parabola in Fig. 4b, which comes from 368 data points, this "estimation-of-parameters criterion" corresponds to an uncertainty of $[S^-]$ of ± 0.0005. (Cf. the lowest horizontal line in Fig. 4b.) It has been known, however, that the $\Delta\chi^2 = 1$ criterion is unrealistic in global analysis when combining data sets with diverse systematic errors from many different experiments [13, 25, 26]; in this circumstance, the overall χ^2 function provides a simple measure of relative goodness-of-fit in the minimization process, but it does not have the strict statistical significance of a pure parameter fitting problem as presented in textbook examples. This estimate of the uncertainty of $[S^-]$ is far too small.

Another often-used method to evaluate "goodness-of-fit" is to apply the *cumulative distribution function* P for the χ^2 distribution. One considers unacceptable values of χ^2 greater than χ^2_{68} (or χ^2_{90}) where $P(\chi^2 < \chi^2_f) = f$. For 386 data points, the 68% (90%) criterion corresponds to $\chi^2/\chi^2_{\rm min} = 1.033$ (1.1) respectively. These two criteria are represented by the two upper horizontal lines in Fig. 4b. The uncertainty ranges of $[S^-]$ for these two cases are ± 0.002 (0.003) respectively.

[13] These difficulties, and practical methods to handle them, are discussed in detail in [13, 25, 26].

The extensive studies on quantifying uncertainties in the global analysis context [13,25,26] suggest that for this case a realistic range should be somewhere between the two extreme cases shown in Fig. 4b. Hence we adopt the uncertainty range $0 < [S^-] < 0.004$ by this analysis, which corresponds to the middle horizontal line in the graph (or the χ^2_{68} criterion). Whereas a very small strangeness asymmetry, consistent with zero, is not ruled out by this criterion, large negative values of $[S^-]$ (such as -0.0027, cited in [12]) are strongly disfavored; cf. also Table 1. Additional sources of uncertainty will be discussed in the following section.

4.5 Additional sources of uncertainty

We have performed three series of studies to further assess the robustness of our main results. These will help us to determine a better estimate of the overall uncertainty of $[S^-]$.

Pure leading order fits

Since the experimental analyses of the CCFR-NuTeV dimuon data have been done in LO QCD [1, 12], we have carried out a whole series of purely LO global analyses, following the same procedures as outlined above, in order to provide a basis for comparison. The results can be summarized as follows.

(1) The overall χ^2 for the global fit increased by ~ 200 over the comparable fits described above; while the χ^2's for the dimuon data sets actually decreased slightly. This is not surprising, since the current state of global analysis, with precision data from many experiments, requires the use of NLO QCD theory – in particular for the collider data with typically large perturbative corrections. On the other hand, the new dimuon data still have comparably large experimental errors and the NLO corrections are small $[\mathcal{O}(\lesssim 20\%)]$, such that an LO fit is adequate for them.

(2) We explored the allowed range of strangeness asymmetry $[S^-]$ in this LO study under different assumptions on the $x \to 0$ and $x \to 1$ behavior of the $s^+(x)$ and $s^-(x)$ functions. First, we found that the dependence of χ^2_{dimuon} on $[S^-]$ is generally parabolic, rather similar to Fig. 4. The width of the distribution is comparable to Fig. 4. The central value for $[S^-]$ is within the range $(0, 0.0015)$; the exact value depends on the $x \to 0$ and $x \to 1$ behavior of $s^\pm(x)$ assumed.

(3) We also found that the $\chi^2_{\text{inclusive I}}$ versus $[S^-]$ curve, while generally flatter, does "flop around" enough for the cases studied so that no clear pattern can be discerned. The specific shape of this curve shown in Fig. 3 is not a common characteristic of these fits.

Charm mass dependence

The CCFR-NuTeV dimuon analysis treated the charm mass as one of the fit parameters. Their analyses favored a rather high value of $m_c = 1.6\,\text{GeV}$ (compared to, e.g., the PDG estimate of $1.0\,\text{GeV} < m_c < 1.4\,\text{GeV}$). The CTEQ global analyses are usually done with a fixed value of $m_c = 1.3\,\text{GeV}$. To see whether the comparison between our results is strongly influenced by the choice of the charm mass, we have performed several series of fits with m_c varying from 1.3 GeV to 1.7 GeV. Again, the general features, as described above, stay the same. The central value of $[S^-]$ does vary with the choice of m_c within a given series of fits, but the pattern is not universal. The range over which the central value wanders is of the order ~ 0.0015, comparable to the width of the parabola in Fig. 4. Unlike the specific analysis of CCFR-NuTeV, the overall χ^2 for the global analysis does favor a lower value of m_c.

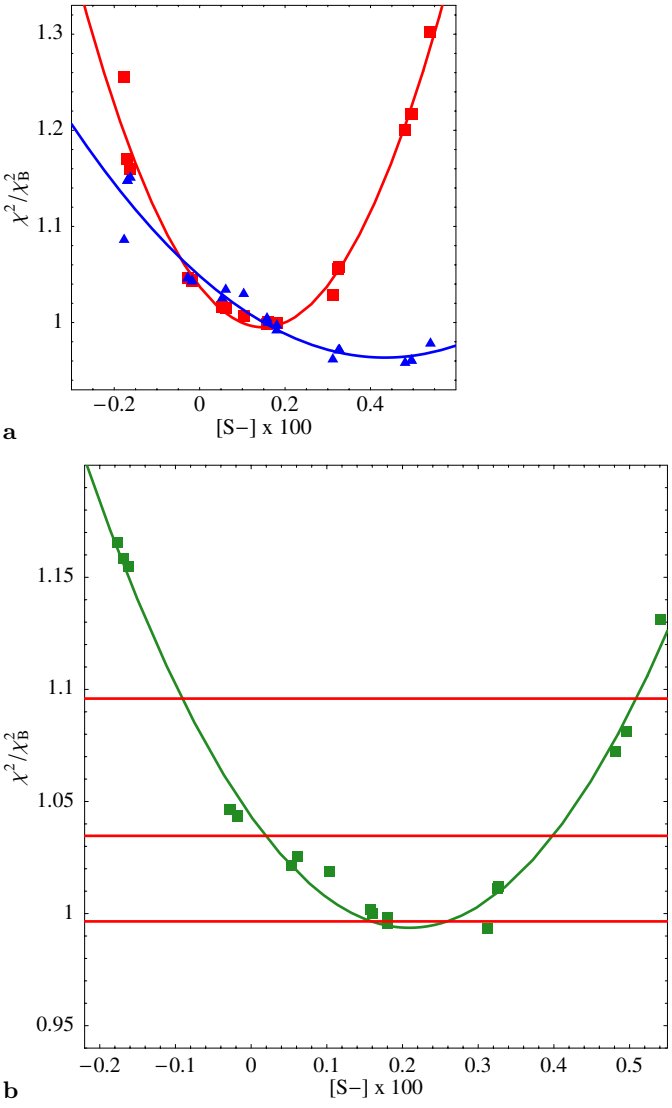

Fig. 4. Values of χ^2/χ^2_B versus $[S^-]$ by the Lagrange multiplier method in global analysis. Panel **a** shows the dimuon data sets (■) and the "Inclusive I" data sets (▲) separately, and **b** shows these data sets combined (■). (Cf. text and Table 1)

Dependence on decay and fragmentation model

To estimate the dependence of our results on the model used to convert the measured dimuon cross sections to structure functions for charm production, we repeated our analyses using an alternative conversion table, provided by the CCFR-NuTeV collaboration.[14] This alternative table is based on Buras–Gaemers PDFs used in CCFR-NuTeV analyses with Collins–Spiller fragmentation functions. It is similarly tuned to detailed features of the measured dimuon cross sections as that described in Sect. 4.2.[15] The results obtained from the alternative fits are, again, similar to those described earlier. The $\chi^2_{\rm dimuon}$ versus $[S^-]$ parabola generally has the same width as in Fig. 4. The central value for $[S^-]$ is in the range $0 < [S^-] < 0.0015$ – in the lower half of the range quoted at the end of Sect. 4.4. The dependence of $\chi^2_{\rm inclusive\ I}$ on $[S^-]$ shows no definitive trend.

Taken together, the results of the additional studies described in these three paragraphs lead to several conclusions.
(i) The general features described in Sects. 4.3 and 4.4 are robust;
(ii) the central value of $[S^-]$ wanders around within a range that is consistent with the width of the $\chi^2_{\rm dimuon}$ versus $[S^-]$ parabola, and
(iii) these additional results do not significantly change the estimates of the previous section, except to shift the central estimated value of $[S^-]$ to a slightly lower value, and to extend the range of uncertainty on the lower side somewhat. The envelope of these additional uncertainties provides an estimated range of uncertainty of the strangeness asymmetry of[16]

$$-0.001 < [S^-] < 0.004\ . \qquad (16)$$

This large range reflects both the limit of current experimental constraints and the considerable theoretical uncertainty, as explicitly discussed in the text. The theoretical uncertainties can be reduced in a refined NLO analysis; the results remain to be seen. The limitations on the experimental constraints will remain, until new experiments are done.

5 Comparisons to previous studies

A comprehensive global QCD analysis with emphasis on the strangeness sector has been carried out previously by BPZ [4].[17] Without the dimuon data, which are directly sensitive to strangeness, the results of BPZ implicitly rely on small differences between large neutral- and charged-current inclusive cross sections from different experiments. The latest representative $s^-(x)$ and $S^-(x)$ functions extracted by BPZ are shown in Fig. 1, along with our reference fit B. The main feature of the BPZ curves is a positive bump at rather large x.[18] This feature has been attributed to the influence of the CDHSW data, particularly when re-analyzed at the cross section level along with the other DIS experiments. Their conclusion that the data favor a positive value of the momentum integral $[S^-]$ is in general agreement with our detailed study based on the LM method. However, the different shapes of $s^-(x)$ seen in Fig. 1 clearly underline the difference in inputs:
(i) our results are mainly dictated by the CCFR-NuTeV dimuon data (which are not present in the BPZ analysis);
(ii) their results rely on a delicate analysis of DIS cross-section data (not matched in our structure function analysis), and
(iii) the difference in flexibility of the parametrizations of the non-perturbative input functions can influence the results.

The CCFR and NuTeV collaborations performed separate and combined analyses of s and $\bar{s}$ [1], based on their own dimuon and inclusive cross sections. To parameterize the $s(x)$ and $\bar{s}(x)$ distributions, they chose the model formula

$$\begin{pmatrix} s(x,Q) \\ \bar{s}(x,Q) \end{pmatrix} = \frac{\bar{u}(x,Q)+\bar{d}(x,Q)}{2} \begin{pmatrix} \kappa(1-x)^{\alpha} \\ \bar{\kappa}(1-x)^{\bar{\alpha}} \end{pmatrix} \qquad (17)$$

for all $\{x, Q\}$, where $\kappa, \bar{\kappa}, \alpha, \bar{\alpha}$ are fitting parameters.

Curves representing the general behavior of the model (17) at $Q^2 = 10\,\mathrm{GeV}^2$, with parameter values $(\kappa, \bar{\kappa}, \alpha, \bar{\alpha})$ taken from [1], have been shown in Fig. 1 for comparison with the other distributions. While this model might be acceptable for a limited range of x and Q, it leads to problems when extrapolated to general $\{x, Q\}$ values:
(i) the strangeness number sum rule $[s^-] = 0$ is violated (in fact, the integral $[s^-]$ diverges unless $\kappa = \bar{\kappa}$), as is the momentum sum rule, (6);
(ii) the QCD evolution equations are violated by the Q-dependent paramaterizations of the PDFs.[19] The first problem is evident in Fig. 1.[20]

It could be argued that, since the experiment only covers a limited range of x, the enforcement of the sum rules is not critical in extracting limited information on $s(x, Q)$

[14] We thank Kevin MacFarland for supplying this table.
[15] However, since our CTEQ6-like PDFs are rather different from the CCFR Buras–Gaemers PDFs, it is not clear how good the approximation is to use this conversion table. That is, the self-consistency of the procedure is not assured.
[16] The uncertainties from the various sources need not be combined in quadrature, because they are not statistically independent sources, but rather systematic uncertainties of the theory.
[17] As mentioned in Sect. 4, BPZ work directly with DIS cross sections (instead of structure functions), with detailed attention to systematic errors and other sources of uncertainties.
[18] The BPZ curve displayed includes the more recent analysis "with CCFR (inclusive data)." The original "without CCFR" solution in [4] has a more pronounced large x bump and a smaller negative region. An $s^-(x)$ function of such magnitude at large x is in disagreement with the CCFR-NuTeV analysis; in addition, it would make $s(x)$ and $\bar{s}(x)$ behave quite differently compared with the non-strange sea quarks and the gluon, i.e., $\sim (1-x)^p$, with p in the range 5–10.
[19] These problems are independent of the specific issues of the strange quark asymmetry.
[20] Re-analysis of the CCFR-NuTeV data by the experimental group, taking into account these issues, are underway. Initial results from partial implementations of the above-mentioned theoretical constraints were reported by [29].

Table 2. The coefficients of the "standard fit" (B-fit) described in Sect. 4.3

B-fit	A_0	A_1	A_2	A_3	A_4	A_5
d_v	1.55891	0.62792	5.08865	0.70688	−0.26338	3.00000
u_v	1.73352	0.55260	2.90090	−2.63846	1.45774	1.85987
g	31.24912	0.52014	2.38230	4.23010	2.33765	−3.00000
$\bar{d}/\bar{u}$	–	10.23811	5.19599	14.85860	17.00000	8.68941
$\bar{u}+\bar{d}$	0.06758	−0.29681	7.71700	−0.82223	4.43481	0.66711
$s+\bar{s}$	0.04966	0.03510	7.44149	−1.44570	5.13400	0.59659
$s-\bar{s}$	−0.08438	0.18803	2.36708	0.04590	0.00000	0.00000

and $\bar{s}(x,Q)$. Given this, the CCFR curve in Fig. 1 implies negative $s^-(x)$ over most of the experimental x range (0.01–0.3).[21] The uncertainty is smaller at the lower x end because of better statistics. It is this feature of the data that we invoked in the general discussion of Sect. 2.

To describe the behavior of $s^-(x)$ over the full x range, the strangeness number sum rule must be enforced. The sum rule also provides a powerful theoretical constraint on the data analysis, as demonstrated in Sects. 2 and 4. For functions to be candidate *universal* parton distributions of the pQCD formalism, they must satisfy both the sum rules and the QCD evolution equations.

6 Conclusion

We find a range of solutions in the strangeness sector that are consistent with all relevant world data used in the global analysis. The dimuon data are vital in constraining the strangeness asymmetry parameters. The constraints provided by other inclusive measurements, labeled as "inclusive I" in the text, are consistent with those provided by dimuon data, although much weaker. The allowed solutions generally prefer the momentum integral $[S^-] \equiv \int_0^1 x[s(x)-\bar{s}(x)]\,\mathrm{d}x$ to be positive. This conclusion is quite robust, and it follows from the basic properties of pQCD and from qualitative features of the experimental data. However, the size of this strangeness momentum asymmetry is still quite uncertain; we can only estimate that $[S^-]$ lies in the range from -0.001 to $+0.004$. The Lagrange multiplier method explicitly demonstrates that both the dimuon data and the "inclusive I" data sets strongly disfavor a large negative value of $[S^-]$, although they may still be consistent with zero asymmetry.

The fact that $[S^-]$ has a large uncertainty has significant implications for the precision measurement of the weak mixing angle, $\sin^2\theta_{\mathrm{W}}$, from neutrino scattering. This issue is studied separately in [8].

This paper marks the first global QCD analysis incorporating direct experimental constraints on the strangeness sector. We have so far focused only on the strangeness asymmetry, which represents a new frontier in parton degrees of freedom. Much still needs to be done to improve the treatment of the dimuon data (to true NLO accuracy), and to fully explore all the degrees of freedom associated with $s^+(x)$ and $s^-(x)$. As progress is made on these fronts, the uncertainty on $[S^-]$ will no doubt decrease as well.

[21] This is consistent with the fact that (without the constraint of sum rules) [12] quotes $[S-] = -0.0027 \pm 0.0013$.

Note added. After this manuscript was completed an investigation of the 3-loop perturbative strangeness asymmetry was presented in [27].

Acknowledgements. We thank members of the CCFR and NuTeV collaboration, in particular T. Bolton and M. Goncharov, for discussions of the dimuon data, and assistance in their use, and Kevin MacFarland, Dave Mason and Panagiotis Spentzouris for useful comments and suggestions. We also thank Benjamin Portheault for discussions of the BPZ work and for assistance in generating their results for comparison. F.O. acknowledges the hospitality of MSU and BNL where a portion of this work was performed. This research was supported by the National Science Foundation (grant No. 0100677), RIKEN, Brookhaven National Laboratory, and the U.S. Department of Energy (Contract No. DE-AC02-98CH10886, and No. DE-FG03-95ER40908), and by the Lightner-Sams Foundation.

Appendix

In this appendix, we provide some detailed information on the parametrization of the non-perturbative parton distribution functions used in our global analysis work, as well as the values of the parameters for the representative fits.

The non-strange parton distributions at $Q = Q_0 = 1.3\,\mathrm{GeV}$ are parametrized as in CTEQ6. We use

$$x\,f(x,Q_0) = A_0\,x^{A_1}\,(1-x)^{A_2}\,\mathrm{e}^{A_3 x}\,(1+\mathrm{e}^{A_4}x)^{A_5} \qquad (18)$$

with independent parameters for parton flavor combinations $u_v \equiv u-\bar{u}$, $d_v \equiv d-\bar{d}$, g, and $\bar{u}+\bar{d}$. To distinguish the $\bar{d}$ and $\bar{u}$ distributions, we parametrize the *ratio* $\bar{d}/\bar{u}$, as a sum of two terms:

$$\begin{aligned}&\bar{d}(x,Q_0)/\bar{u}(x,Q_0) \qquad (19)\\ &= A_1\,x^{A_2}\,(1-x)^{A_3} \;+\; (1+A_4\,x)\,(1-x)^{A_5}\;.\end{aligned}$$

The strangeness sector is parametrized according to the description of Sect. 3 with

$$x s^+(x,Q_0) = A_0\,x^{A_1}\,(1-x)^{A_2}\,\mathrm{e}^{A_3 x}\,(1+\mathrm{e}^{A_4}x)^{A_5},$$

Table 3. Coefficients for A-, C- and $B^{+,-}$ fit

A-fit	A_0	A_1	A_2	A_3	A_4	A_5
d_v	1.55485	0.62740	5.09550	0.70010	−0.25130	3.00000
u_v	1.73345	0.55260	2.90090	−2.63740	1.45810	1.85910
g	31.05518	0.51840	2.38230	4.24730	−2.33790	3.00000
$\bar{d}/\bar{u}$	–	10.23920	5.19690	14.85860	17.00000	8.68530
$\bar{u}+\bar{d}$	0.06677	−0.29810	7.71700	−0.80540	4.45630	0.66420
$s+\bar{s}$	0.05133	0.06567	7.59880	−1.43972	5.13400	0.61715
$s-\bar{s}$	−0.02000	−0.06562	−0.48403	0.01987	−0.58837	0.00000
C-fit	A_0	A_1	A_2	A_3	A_4	A_5
d_v	1.39587	0.60594	4.75379	−0.75291	0.31387	3.00000
u_v	1.72080	0.55260	2.90090	−2.36331	1.60950	1.59812
g	29.40547	0.50423	2.38230	4.41409	2.34266	−3.00000
$\bar{d}/\bar{u}$	–	10.23202	5.19618	14.85860	17.00000	8.62620
$\bar{u}+\bar{d}$	0.06479	−0.30038	7.71700	−0.68604	4.61325	0.62988
$s+\bar{s}$	0.04289	0.00809	7.71700	−1.22365	5.13400	0.62988
$s-\bar{s}$	−2.36926	0.99191	8.23499	0.07884	0.00000	0.00000
B^+-fit	A_0	A_1	A_2	A_3	A_4	A_5
d_v	1.43611	0.61170	4.73270	−0.67420	0.24920	3.00000
u_v	1.71921	0.55260	2.90090	−2.39220	1.60430	1.61490
g	29.76781	0.50800	2.38230	4.35570	−2.33860	3.00000
$\bar{d}/\bar{u}$	–	10.19560	5.16810	14.85860	17.00000	8.69760
$\bar{u}+\bar{d}$	0.06729	−0.29650	7.71700	−0.75670	4.52290	0.64380
$s+\bar{s}$	0.03456	0.00210	8.23420	−1.26970	5.13410	0.72501
$s-\bar{s}$	−0.40480	0.22103	3.40190	0.04701	0.31550	0.00000
B^--fit	A_0	A_1	A_2	A_3	A_4	A_5
d_v	1.43611	0.61170	4.73270	−0.67420	0.24920	3.00000
u_v	1.71921	0.55260	2.90090	−2.39220	1.60430	1.61490
g	29.76781	0.50800	2.38230	4.35570	−2.33860	3.00000
$\bar{d}/\bar{u}$	–	10.19560	5.16810	14.85860	17.00000	8.69760
$\bar{u}+\bar{d}$	0.06717	−0.29650	7.71700	−0.75670	4.52290	0.64380
$s+\bar{s}$	0.04356	0.00210	7.33918	−1.26970	5.13400	0.60083
$s-\bar{s}$	0.01781	0.22103	−15.02691	0.22693	−1.23666	0.00000

where the $A_{1,2,3,4,5}$ coefficients are either equated to those of $\bar{u}+\bar{d}$, or allowed to vary independently, depending on the particular fit being performed, and

$$s^-(x,Q_0) = s^+(x,Q_0)$$
$$\times \tanh\left[A_0\, x^{A_1}(1-x)^{A_2}\left(1-\frac{x}{A_3}\right)\left(1+A_4\ x+A_5\ x^2\right)\right].$$

As an example, the "standard fit" (B-fit) described in Sect. 4.3 has the coefficients of Table 2.

The other sample fits have coefficients as in Table 3.

References

1. M. Goncharov et al., CCFR and NuTeV Collab., Phys. Rev. D **64**, 112006 (2001); M. Tzanov et al., NuTeV Collab. hep-ex/0306035
2. S.J. Brodsky, B.-Q. Ma, Phys. Lett. B **381**, 317 (1996); A.I. Signal, A.W. Thomas, Phys. Lett. B **191**, 205 (1987); F.G. Cao, A.I. Signal, Phys. Lett. B **559**, 229 (2003); M. Wakamatsu, Phys. Rev. D **67**, 034005 (2003), and references therein
3. G.P. Zeller et al., NuTeV Collab., Phys. Rev. Lett. **88**, 091802 (2002)
4. V. Barone, C. Pascaud, F. Zomer, Eur. Phys. J. C **12**, 243 (2000); this analysis is currently being updated and early results have been presented by B. Portheault at DIS03; http://www.desy.de/dis03. The "BPZ with CCFR" curves in Fig. 1 are from the updated results
5. S. Davidson, S. Forte, P. Gambino, N. Rius, A. Strumia, JHEP **0202**, 037, (2002)
6. K.S. McFarland, S.-O. Moch, hep-ph/0306052
7. P. Gambino, hep-ph/0211009; A. Strumia, hep-ex/0304039
8. S. Kretzer et al., Phys. Rev. Lett. **93**, 041802 (2004)
9. P. Gambino, Int. J. Mod. Phys. A **19**, 808 (2004) [hep-ph/0311257]
10. R.S. Thorne, Int. J. Mod. Phys. A **19**, 1074 (2004) [hep-ph/0309343]
11. H. Abramowicz et al., CDHSW Collab., Z. Phys. C **15**, 19 (1982); C. Foudas et al., CCFR Collab., Phys. Rev. Lett.

64, 1207 (1990); B. Strongin et al., Phys. Rev. D **43**, 2778 (1991); S.A. Rabinowitz et al., CCFR Collab., Phys. Rev. Lett. 70, 134 (1993); A.O. Bazarko et al., CCFR Collab., Z. Phys. C 65, 189 (1995); P. Vilain et al., CHARM II Collab., Eur. Phys. J. C **11**, 19 (1999); P. Astier et al., NOMAD Collab., Phys. Lett. B **486**, 35 (2000)
12. G.P. Zeller, NuTeV Collab., Phys. Rev. D **65**, 111103 (2002); D **67**, 119902 (2003) (E); K.S. McFarland et al., Proceedings of 16th Les Rencontres de Physique de la Vallee d'Aoste: Results and Perspectives in Particle Physics, La Thuile, Aosta Valley, Italy, 3–9 March 2002, hep-ex/0205080
13. J. Pumplin, D.R. Stump, J. Huston, H.L. Lai, P. Nadolsky, W.K. Tung, JHEP **0207**, 012 (2002)
14. A.D. Martin, R.G. Roberts, W.J. Stirling, R.S. Thorne, Eur. Phys. J. C **23**, 73 (2002)
15. M. Glück, E. Reya, A. Vogt, Eur. Phys. J. C **5**, 461 (1998)
16. P. Berge et al., Z. Phys. C **49**, 187 (1991)
17. M. Glück, S. Kretzer, E. Reya, Phys. Lett. B **380**, 171 (1996); B **405**, 391 (1996) (E)
18. R.M. Barnett, Phys. Rev. Lett. **36**, 1163 (1976)
19. T. Gottschalk, Phys. Rev. D **23**, 56 (1981)
20. S. Kretzer, I. Schienbein, Phys. Rev. D **58**, 094035 (1998)
21. M.A.G. Aivazis, F.I. Olness, W.K. Tung, Phys. Rev. Lett. **65**, 2339 (1990)
22. S. Kretzer, M.H. Reno, Phys. Rev. D **69**, 034002 (2004)
23. M. Glück, S. Kretzer, E. Reya, B **398**, 381 (1997); B **405**, 392 (1997) (E)
24. S. Kretzer, D. Mason, F.I. Olness, Phys. Rev. D **65**, 074010 (2002)
25. J. Pumplin, D.R. Stump, W.K. Tung, et al., Phys. Rev. D **65**, 014011 (2002); D **65**, 014013 (2002); D **65**, 014012 (2002)
26. A.M. Cooper-Sarkar, J. Phys. G **28**, 2669 (2002) [hep-ph/0205153]; also http://www-zeuthen.desy.de/~moch/heralhc/gwenlan-coopersarkar.pdf
27. S. Catani, D. de Florian, G. Rodrigo, W. Vogelsang, Phys. Rev. Lett. **93**, 152003 (2004)
28. K. MacFarland, P. Spentzouris, communications at the LP03 Symposium and WIN03 Workshop
29. P. Spentzouris at International Workshop on Weak Interactions and Neutrinos 2003 (WIN03), Lake Geneva, October, 2003